UHASSELT
KNOWLEDGE IN ACTION

Maastricht University

Faculty of Medicine and Life Sciences
School for Life Sciences
Master of Biomedical Sciences

Master's thesis

Pyridoxamine limits cardiac dysfunction after doxorubicin chemotherapy and does not affect doxorubicin efficacy on rat mammary tumor cells

Eline Verghote

Thesis presented in fulfillment of the requirements for the degree of Master of Biomedical Sciences, specialization Molecular Mechanisms in Health and Disease

SUPERVISOR :

Prof. dr. Virginie BITO

MENTOR :

De heer Sibren HAESEN

2022
2023

Transnational University Limburg is a unique collaboration of two universities in two countries: the University of Hasselt and Maastricht University.

UHASSELT
KNOWLEDGE IN ACTION

www.uhasselt.be
Universiteit Hasselt
Campus Hasselt:
Martelarenlaan 42 | 3500 Hasselt
Campus Diepenbeek:
Agoralaan Gebouw D | 3590 Diepenbeek

Faculty of Medicine and Life Sciences
School for Life Sciences
Master of Biomedical Sciences

Master's thesis

Pyridoxamine limits cardiac dysfunction after doxorubicin chemotherapy and does not affect doxorubicin efficacy on rat mammary tumor cells

Eline Verghote

Thesis presented in fulfillment of the requirements for the degree of Master of Biomedical Sciences, specialization Molecular Mechanisms in Health and Disease

SUPERVISOR :

Prof. dr. Virginie BITO

MENTOR :

De heer Sibren HAESEN

Pyridoxamine limits cardiac dysfunction after doxorubicin chemotherapy and does not affect doxorubicin efficacy on rat mammary tumor cells*

Verghote E[1], Haesen S[1], Deluyker D[1], Bito V[1]

[1]Cardio and Organ Systems (COS) research group, Biomedical Research Institute (BIOMED), Hasselt University, Campus Diepenbeek,
Agoralaan Gebouw C - B-3590 Diepenbeek

**Running title: Pyridoxamine is cardioprotective and does not affect the antitumor activity of doxorubicin*

To whom correspondence should be addressed: Virginie Bito, Tel: +32 11 26 92 85 ; Email: Virginie.Bito@uhasselt.be

Keywords: pyridoxamine, cardioprotection, doxorubicin, LA7, breast cancer,

ABSTRACT

Although doxorubicin (DOX) is a highly efficient chemotherapeutic agent against cancer, it displays important dose-dependent toxic effects on the heart (1). The vitamin B6 derivative pyridoxamine (PM) improves cardiac function after DOX. However, the underlying cardioprotective mechanisms of PM and its effect in a cancer setting remain unknown. In this study, we aim to investigate the underlying mechanisms of PM cardioprotection and whether PM antagonizes the antitumor activity of DOX. Female Sprague Dawley rats were treated weekly with 0.9% saline (CTRL), DOX (2 mg/mL), PM (1 g/L), or DOX and PM for eight weeks. DOX increased the gene expression of the pro-inflammatory marker IL-1β (P=0.0047) and the macrophage marker CD68 (P=0.0279). The M2a macrophage marker CD163 was upregulated after DOX (P=0.0019). DOX-treated animals showed increased lipid peroxidation (P=0.0288) and mitochondrial damage characterized by vacuolization and disrupted cristae. PM treatment reduced CD68 (P=0.0449) and CD163 (P=0.0254), and prevented mitochondrial damage. Finally, *in vitro* experiments showed a reduction in LA7 cell viability (P<0.0001) and proliferation (P=0.005 and P<0.0001) after acute exposure to DOX (1 µg/mL). This was associated with increased levels of cleaved caspase-3 (P=0.0002). Importantly, concomitant treatment with PM (100 µM) did not alter these parameters. In conclusion, PM is cardioprotective after DOX by reducing macrophage upregulation and mitochondrial damage. PM does not antagonize the antitumor effects of DOX, which is promising for cancer patients suffering from cardiotoxicity. Whether PM is also an effective cardioprotective treatment in a preclinical cancer model in combination with DOX treatment requires further investigation.

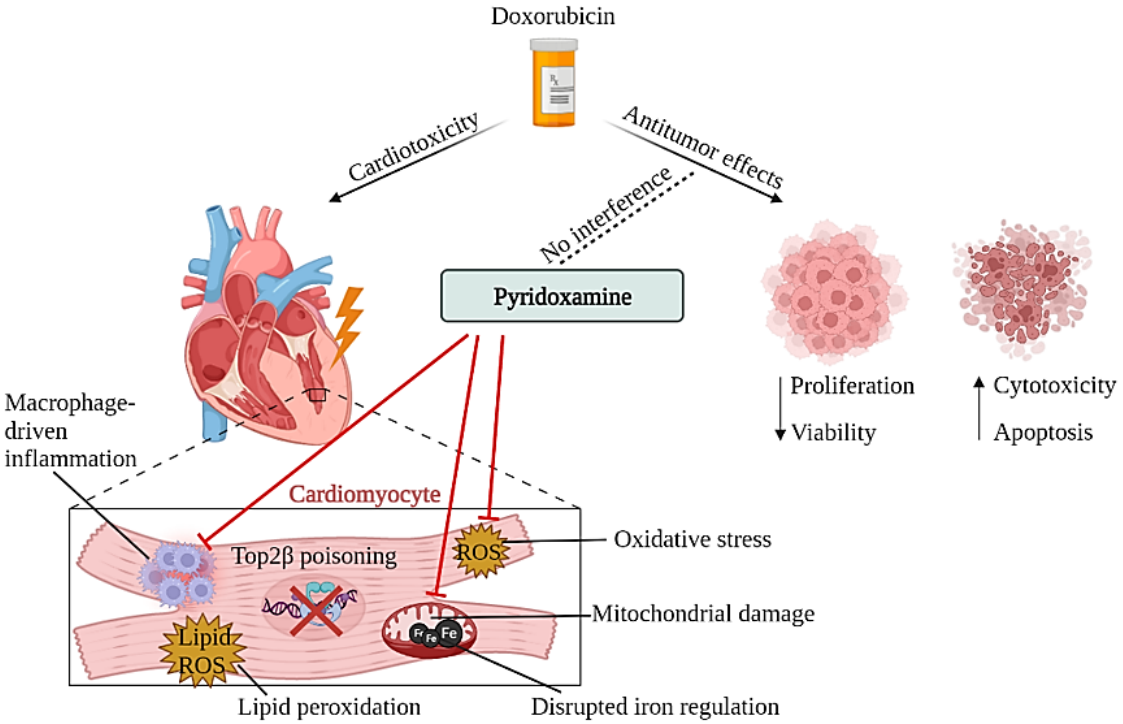

Graphical abstract. Top2β: topoisomerase 2 beta, ROS: reactive oxygen species

INTRODUCTION

The rise in cancer survivors is associated with the adverse effects of anticancer treatments

Worldwide, breast cancer is the most frequent cancer in women and the fifth leading cause of cancer-related deaths (2-4). Each year, more than 2 million women are diagnosed with breast cancer (2, 4). Over the last decades, breast cancer prognosis has dramatically improved. Currently, the overall 5-year survival is more than 90%, and the overall 10-year survival is approximately 80%, leading to an increased cancer survivor population (5). These improvements are mainly due to earlier diagnosis through screening programs (e.g., routine mammography) and treatment advances (e.g., chemotherapy, immunotherapy, targeted therapy). However, some of these therapeutic agents are associated with life-threatening short-term and long-term adverse effects (5).

The dark side of chemotherapy: cardiotoxicity

Anthracyclines are a class of chemotherapeutic agents that maintain a prominent role in the treatment of many cancers, including breast cancer. Approximately 32% of breast cancer patients receive anthracycline chemotherapy (1). The most important anthracycline is doxorubicin (DOX) with a success rate of 54% (6). However, DOX is associated with dose-dependent cardiotoxicity, which can manifest during treatment or years after treatment completion (1, 7, 8). In clinics, patients receive cumulative doses of DOX ranging from 350-450 mg/m^2, corresponding to a cardiotoxicity incidence of ±33%, of which 5% develops heart failure (HF). Nevertheless, this HF incidence can rise exponentially to 48% at a dose of 650 mg/m^2, administered in case of advanced breast cancer (1, 9). In addition, more than 20% of mortality among breast cancer survivors is attributed to HF, which is as high as the cancer mortality itself, and is, therefore, a major concern in the field of cardio-oncology (10). Thus, it is important to evaluate the cardiotoxic effects after DOX treatment in these cancer patients.

Mechanisms of DOX-induced cardiotoxicity

Dilated cardiomyopathy (DCM) has been described as the major outcome following DOX chemotherapy (11). DCM is a progressive disease of the heart muscle, characterized by an enlarged left ventricle (LV), weakened heart muscle, and a decline in LV ejection fraction (LVEF) of ≥10% (12, 13). In the pathogenesis of DOX-induced cardiotoxicity, DNA topoisomerase 2 beta (Top2β) poisoning, oxidative stress, iron accumulation, mitochondriopathy and

inflammation, ultimately leading to cardiomyocyte apoptosis, play an important role. In cancer cells, DOX hampers DNA transcription and replication by inhibiting the topoisomerase 2 alfa (Top2α) activity. As a result, the cancer cells are committed to apoptosis. Nevertheless, DOX also targets the isoform Top2β, expressed in cardiomyocytes, leading to cardiomyocyte apoptosis (14, 15). Another clear subcellular target of DOX is the mitochondria, which are highly abundant in cardiomyocytes. At this site, DOX can be transformed to reactive oxygen species (ROS) by the ROS-producing enzymes mitochondrial NADH dehydrogenase and microsomal NADPH-P450 reductase, resulting in oxidative stress (15). In addition, it has been reported that DOX interacts with the iron regulatory proteins (IRP), which regulate the expression of genes involved in iron metabolism, thereby disrupting the iron homeostasis in the heart. Indeed, DOX increases intracellular iron uptake, especially in the mitochondria, and storage, without changing iron export, resulting in iron accumulation. DOX also has the ability to bind directly to iron (Fe^{3+}) to form unstable DOX-Fe^{3+} complexes intracellular. This complex reduces Fe^{3+} to Fe^{2+} and oxidizes DOX to a free radical, associated with increased ROS production. ROS react with membrane lipids and induce lipid peroxidation, generating lipid radicals (16, 17). Both iron accumulation and lipid peroxidation are key events in ferroptosis, a non-apoptotic iron-dependent form of cell death (17-19). Furthermore, DOX has a high affinity with cardiolipin, a phospholipid abundant in the inner mitochondrial membrane, which lead to the formation of DOX-cardiolipin complexes, resulting in mitochondrial dysfunction (15, 20). One of the major signaling pathways activated in response to oxidative stress is the NF-κB pathway, which regulates the expression of genes involved in inflammation, oxidative stress, and apoptosis. Depending upon the cell type, NF-κB activation either promotes or blocks apoptotic cell death (18). It has been reported that inhibition of NF-κB activation sensitizes cancer cells to DOX-induced apoptosis, indicating anti-apoptotic effects of NF-κB in cancer cells (21). Conversely, NF-κB activation, mediated by DOX-induced H_2O_2, displays a pro-apoptotic role in DOX-treated cardiomyocytes (21). Moreover, DOX-induced cardiac inflammation and fibrogenesis are observed through the upregulation of NF-κB, implicating the role of NF-κB in DOX-induced cardiac injury (22).

The problem of DOX-induced cardiotoxicity remains without a solution

Alternatively to DOX, analogs of anthracyclines (e.g., epirubicin, idarubicin and daunorubicin) are used in the clinic, supposed to be less cardiotoxic at similar doses of DOX. However, these are known to be less effective and thus higher doses must be given to obtain the same clinical response as DOX, still resulting in cardiotoxicity (20). Additionally, liposomal DOX is used in the clinic to reduce the toxicity profile (23). However, different liposome-encapsulated forms of DOX have been shown to cause important side effects and to be extremely expensive, limiting their clinical use (24). Furthermore, many cardioprotective approaches have been investigated including neurohormonal antagonists, statins, β-blockers, and dexrazoxane (DRZ). To date, DRZ is the only drug approved by FDA for cardioprotection after DOX chemotherapy and has been used for over 30 years in many types of solid and hematological cancers in both adults and children (12). DRZ is an iron-chelating agent, preventing anthracycline-iron complex formation, and inhibits anthracyclines from targeting Top2β, thereby lowering the risk of HF (12, 25). Indeed, DRZ limits cardiac events and the risk of HF in breast cancer patients receiving anthracycline chemotherapy (26). Despite the effectiveness of DRZ, its clinical use has previously been restricted due to interference with the antitumor activity of DOX and the risk of the development of second primary malignancies (27, 28). Moreover, contradicting results about the effect of DRZ on cardiac function and patient prognosis have been reported (29-34). Nevertheless, its supposed interaction with DOX treatment and the risk of second cancers have recently been disapproved. Therefore, the European Medicines Agency removed the restriction on dexrazoxane use in 2017 (30). However, DRZ is only recommended for patients at high risk for cardiotoxicity or who require high doses of anthracyclines (33).

PM offers cardioprotection

Several studies support the view that pyridoxamine (PM), a natural derivate of vitamin B6, might have promising cardioprotective effects in cardiovascular diseases (CVDs) (35). *Jeon and Park (2019)* examined the correlation between dietary vitamin B6 intake and CVD incidence in a prospective cohort study, and observed that a higher intake of vitamin B6 was

associated with a reduced CVD risk in men (36). Moreover, chronic inflammation is a key mechanism underlying CVDs and plasma levels of vitamin B6 are inversely correlated with systemic inflammation markers, suggesting that one of the protective actions of vitamin B6 in CVDs occurs through the suppression of chronic inflammation (37). Indeed, vitamin B6 acts as a co-factor for enzymes that convert kynurenine into metabolites (e.g., kynurenic acid, anthranilic acid, xanthurenic acid, 3-hydroxyanthranilic acid), which exert anti-inflammatory effects (35, 38). In addition, studies have shown that vitamin B6 suppresses inflammation by inhibiting NF-κB activation and NLRP3 inflammasome (35, 38, 39). The NLRP3 inflammasome is activated by the extracellular ATP-stimulated P2X7 receptor (P2X7R) through enhanced ROS production (38). It has evidenced that vitamin B6 directly inhibits P2X7R at physiological levels and suppresses the production of mitochondrial ROS (38). Moreover, vitamin B6 supplementation increases the levels of cardiac imidazole dipeptides (e.g., carnosine, anserine), which are involved in modulating inflammation and oxidative stress, thereby lowering the risk of cardiac injury (38, 40, 41). Thus, these findings indicate that vitamin B6 displays cardioprotective effects through suppressing inflammation and oxidative stress. The beneficial effects of PM in CVDs are also evidenced by our research group in a rat model of myocardial infarction (42). Moreover, we previously showed that PM reduces cardiac impairment after DOX treatment in a tumor-lacking animal model. PM limits the reduction of LVEF (Fig. 1A) and decreases the LV end-systolic volume, which is increased after DOX (Fig. 1B). The cardioprotective mechanisms involve the reduction of inflammation (Fig. 1C), oxidative stress (Fig. 1D) and iron accumulation (Fig 1E-F). These data suggest PM as a potential cardioprotective agent in DOX-induced cardiomyopathy. However, the underlying cardioprotective mechanisms of PM remain poorly understood. Additionally, the effects of PM in a cancer setting are yet to be explored since there is a reciprocal relationship between CVDs and cancer (43). HF and cancer share common risk factors (e.g., aging, smoking, genetic factors, diabetes mellitus) as well as several pathophysiologic mechanisms, including inflammation and oxidative stress. In addition, data have been generated showing that circulating factors secreted from the cancer cells influence the development of HF, and conversely (43-45). Thus, it is important to evaluate the effects of PM in a tumor environment.

In our study, we aim to further unravel the underlying mechanisms of PM cardioprotection, examine whether PM interferes with the antitumor activity of DOX and investigate potential antitumor effects of PM itself. Additionally, we aim to develop a rat mammary tumor model for future DOX cardiotoxicity studies, using the LA7 mammary tumor cell line.

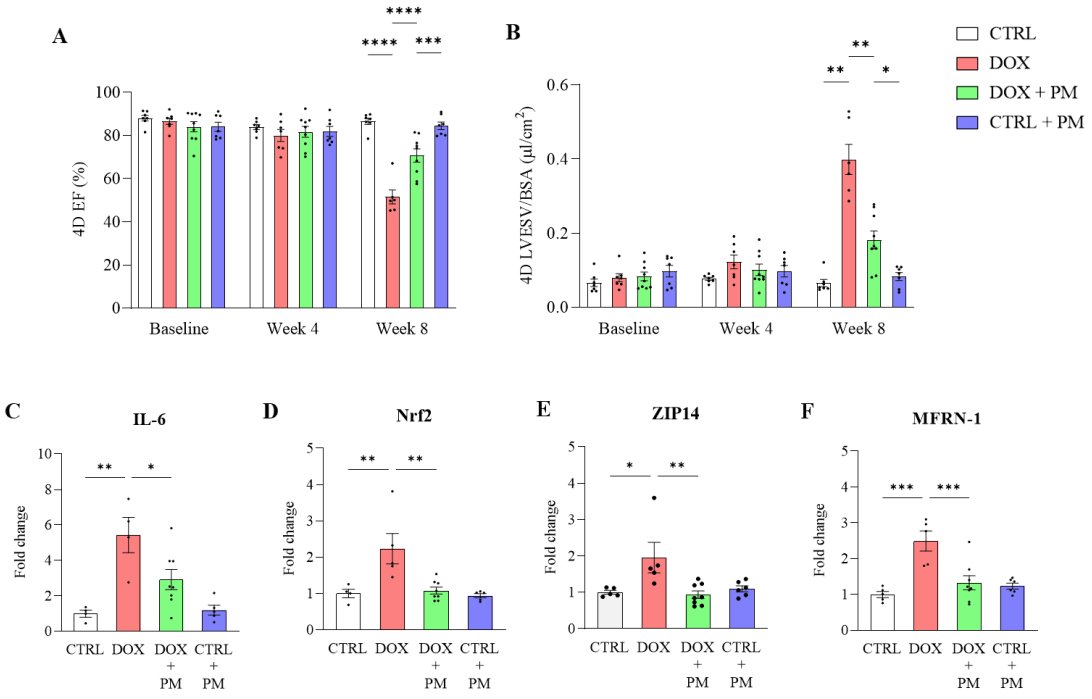

Figure 1: PM limits cardiac dysfunction after eight weeks of DOX treatment. (A-B) Percentage of 4D EF **(A)** and 4D LVESV/BSA **(B)** at baseline, week 4, and week 8 in CTRL (CTRL, N=7), DOX (N=7), DOX+PM (N=9) and PM (N=7) animals. **(C-F)** Gene expression of the pro-inflammatory marker IL-6 **(C)**, the antioxidant transcription factor Nrf2 **(D)**, the cellular iron transporter ZIP14 **(E)** and the mitochondrial iron transporter MFRN-1 **(F)** in CTRL (N=4), DOX (N=5), DOX+PM (N=8) and PM (N=5) animals. Data are presented as mean ± SEM. *P<0.05, **P<0.01, ***P<0.001, ****P<0.0001. EF, ejection fraction. LVESV, left ventricular end-systolic volume. BSA, body surface area Nrf2, nuclear factor erythroid 2–related factor 2. IL-6, interleukin 6. MFRN-1, mitoferrin-1.

EXPERIMENTAL PROCEDURES

Animal experiments – All animal experiments were performed according to the EU Directive 2010/63/EU for animal testing and approved by the local ethical committee (Ethical Commission for Animal Experimentation, UHasselt, Diepenbeek, Belgium, ID 201942). Rats were housed in standard cages with cage enrichment at the conventional animal facility of UHasselt. Rats were maintained under controlled conditions regarding temperature (22°C) and humidity (22–24%). Water and food (2018 Teklad global rodent diet, Harlan, Belgium) were provided *ad libitum.*

Experimental protocol - Healthy female Sprague Dawley rats (N=30, Janvier Laboratories, Le Genest- Saint-Isle, France) were randomly assigned to weekly IV injection with DOX (2 mg/mL, Accord Healthcare B.V., Utrecht, Netherlands) or an equal volume of 0.9% saline (CTRL) for eight weeks. Two extra groups received Pyridoxamine Dihydrochloride (PM, 1 g/l, Santa Cruz Biotechnology Inc., Heidelberg, Germany) *ad libitum* via the drinking water in addition to DOX or saline. The rats were sacrificed by an overdose of sodium pentobarbital (Dolethal, 150 mg/kg IP, Val d' hony Verdifarm, Beringen, Belgium). Hearts were excised. Left ventricular (LV) tissue was fixed in paraformaldehyde (PFA, 4%) and embedded in paraffin. Transverse sections of 7 µm were obtained. Residual LV tissue was crushed to powder for qPCR analysis.

qPCR analysis – Total RNA was extracted from LV tissue according to the manufacturer's guidelines of the RNeasy Fibrous Tissue Mini Kit (Qiagen, Antwerp, Belgium). The quality and purity of the RNA were evaluated using the NanoDrop 2000 spectrophotometer (Isogen Life Science, Tense, Belgium). cDNA was synthesized using the reverse transcription system (Quanta Bioscience, Beverly, United States) and qPCR was performed with the StepOnePlus Real-Time PCR System (Thermo Fisher Scientific). Primers are shown in Table S1. Relative quantification of gene expression was accomplished using the comparative Ct method following the MIQE guidelines (46). Data were normalized to the most stable reference genes determined by GeNorm (Table S1).

Immunohistochemistry (IHC) – LV sections were stained for 4-hydroxynonenal (4-HNE) to assess lipid peroxidation. First, heat-mediated antigen retrieval was performed with citrate buffer (pH = 6). Endogenous peroxidase was blocked with 30% hydrogen peroxide (H_2O_2) for 20 minutes. Sections were permeabilized with 0.05% Triton X100 (Merck Life science BV, Overijse, Belgium) and blocked with serum-free protein block (X0909, Dako, Agilent Technologies, Diegem, Belgium) for 20 minutes. LV sections were incubated overnight at 4°C with a mouse monoclonal primary antibody for 4-HNE (1:400, ab48506, Abcam). The EnVision Detection System (Dako Agilent, anti-rabbit/anti-mouse, K5007) was applied for 30 min at RT. Sections were incubated with 3,3′-Diaminobenzidine (DAB, Dako Agilent), counterstained with hematoxylin, and mounted with Dibutylphthalate Polystyrene Xylene (DPX) medium. Sections without primary antibody served as negative controls. Images were acquired using a Leica MC170 camera connected to a Leica DM2000 LED microscope (Leica Biosystems). The level of staining was assessed in four to eight random fields per section using the color deconvolution plugin in Fiji software and was expressed as % of the total surface area (47). Two operators blinded for group allocation performed the analysis independently.

Transmission electron microscopy (TEM) – LV tissue was processed for TEM to assess cardiomyocyte organization. Tissue was fixed overnight with 2% glutaraldehyde in 0.05M

cacodylate buffer at 4°C, post-fixed in 2% osmium tetroxide and stained with 2% uranyl acetate in 10% acetone. Samples were dehydrated in graded series of acetone and embedded in araldite according to the pop-off method. Ultra-thin sections were cut and mounted on formvar-coated grids, counterstained with uranyl acetate and lead citrate, and were imaged in a Philips EM 208 transmission electron microscope (Philips, Eindhoven, Netherlands). Per animal, five random images were taken at 1200x and 6000x magnification. Mitochondrial density was calculated as the number of mitochondria, measured using the cell counter tool in Fiji, normalized to total cell area (47). The mitochondrial, myofilament, and cytoplasm fractions were measured by grid-point analysis in Fiji, counting every point (distance = 2 µm) at the intersection of horizontal and vertical lines (47). Data were presented as a percentage of points hitting the different structures relative to total grid points. All samples were coded and image analysis was performed single-blinded.

Cell culture – Rat mammary tumor cell line LA7 was purchased (ATCC No CRL2283). Cells were cultured in Dulbecco's modified eagle's medium (DMEM) with 1% L-glutamine (L-glut) and 1% penicillin/streptomycin (P/S) supplemented with 10% fetal calf serum (FCS). Cells were incubated at 37°C in a humidified incubator with a 5% CO_2 atmosphere. For viability and proliferation, cells were seeded at a density of 2000 cells per well in a 96-well plate, whereas 5000 cells were seeded for cytotoxicity. After 24H, different DOX concentrations were added to the medium: 0.5 µg/mL, 1 µg/mL, 1.75 µg/mL, 2 µg/mL, 2.5 µg/mL, 5 µg/mL and 10 µg/mL. To study the effect of PM, the following conditions were added: 1 µg/mL DOX, 1 µg/mL DOX + 100 µM PM and 100 µM PM. LA7 cells cultured in medium were used as negative control.

Cell viability assay – To determine cell viability, the medium of the conditioned cells was replaced with an Alamar Blue solution (1:10, cat# DAL1025, Thermo Fisher) after 24H, 48H, and 72H. Following 4H incubation in the humidified incubator at 37°C, fluorescence was measured with a Plate Reader (Clariostar Plus; BMG Labtech; excitation: 570 nm, emission: 600 nm, gain: 2000). Experiments were performed in triplicate. Data were normalized to the negative control.

Proliferation and cytotoxicity assay – Proliferation and cytotoxicity were studied using the IncuCyte® S3 Live-Cell Analysis System (Sartorius, Schaarbeek, Belgium). For cytotoxicity, the Incucyte® Cytotox Green Reagent (1:40000, Sartorius, Schaarbeek, Belgium) was used. Images were taken every 2H for three days with a 10x lens, and each condition was run in triplicate. The percentage of confluence and the total Cytotox green area (μm^2) for proliferation and cytotoxicity respectively were analyzed using the IncuCyte® SX1 Live-Cell Analysis System (Sartorius, Schaarbeek, Belgium).

Immunocytochemistry (ICC) – LA7 cells were cultured in a 24-well plate on cover clips (100 000 cells/well). After 24H, four different conditions were added: DMEM, DOX (1 µg/mL), PM (100µM) and DOX+PM. After 24H, cells were fixed with 4% paraformaldehyde (PFA) for 20 minutes, permeabilized with 0.05% Triton X100 for 30 minutes, and blocked 1H with serum-free protein block. LA7 cells were incubated overnight at 4°C with cleaved caspase 3 antibody (1:1000, cat#9664S, Cell Signaling Technology), followed by incubation for 1H with secondary antibody (donkey anti-rabbit 555, 1:400, cat#A21430, Thermo Fisher). All antibodies were diluted in 1x PBS. Primary antibody were omitted to test for specificity of secondary antibodies. Nuclei staining was performed with 4',6 diamidino-2-phenylindole (DAPI, Sigma). Slides were mounted in fluorescent mounting medium (Invitrogen). Images were acquired in five random fields per slide using a Leica fluorescence microscope (DM 4000 B LED; 20X) with the Leica Application Suite X software. The corrected total fluorescence was quantified using Fiji software by dividing the integrated density by cell number (47). Two operators blinded for group allocation performed the analysis independently.

Mammary tumor induction – Sprague-Dawley female rats were inoculated with LA7 mammary tumor cells. Tumor volume was measured with a caliper. A detailed description can be found in the Supplementary Materials.

Statistical analysis – Statistical analysis was performed using GraphPad Prism (GraphPad Software, version 9.5.0, San Diego, CA, USA). Normal distribution of data was assessed with the D'Agostino & Pearson normality test or the

Shapiro-Wilk test when N<8. For normally distributed data, a parametric one-way or two-way ANOVA for repeated measurements with the Bonferroni post hoc test was used. When data were not normally distributed, the non-parametric Kruskal-Wallis test and the Dunn's multiple comparison test were used. If the standard deviations were not equal, a Brown-Forsythe test with the post hoc Dunnett correction was performed. All data are expressed as mean ± standard error of the mean (SEM). Outliers (ROUT method, Q=1%) were excluded. A value of P<0.05 was considered statistically significant.

RESULTS

PM limits macrophage upregulation and mitochondrial damage after DOX – To unravel the underlying mechanisms of PM cardioprotection against DOX-induced cardiotoxicity, gene expression levels related to macrophage phenotypes were analyzed. As shown in Fig. 2A and B, DOX significantly increased the pro-inflammatory marker IL-1β (P=0.0047) and the expression of the macrophage marker CD68 (P=0.0279), confirming the involvement of macrophages in DOX inflammation. However, no significant difference was observed in the expression of type 1 macrophage marker (M1) CD86 after eight weeks of DOX treatment (Fig. 2C). Furthermore, the gene expression of type 2a macrophage markers (M2a) CD163 and CD206 were assessed. DOX significantly increased the expression of CD163 (P=0.0019) (Fig. 2D). However, the CD206 expression was not significantly altered between the groups (Fig. S1). Interestingly, concomitant treatment with PM significantly reduced the expression of CD68 (P=0.0449), but is still significantly different from PM alone (p=0.0025; Fig. 2B). CD163 levels were also significantly decreased after PM treatment (P=0.0254; Fig. 2D). In addition, 4-HNE content in LV tissue was assessed to examine the role of lipid peroxidation in cardiac dysfunction by DOX. Representative images from CTRL, DOX, DOX and PM, and PM groups are illustrated in Fig. 2E. Quantification of 4-HNE deposition revealed that lipid peroxidation was significantly increased in DOX-treated animals compared to CTRL animals (P=0.0288; Fig. 2F). PM treatment did not ameliorate this parameter. To investigate mitochondrial damage, TEM of LV tissue was performed. Fig. 2G illustrates representative images of mitochondria in LV cardiomyocytes from CTRL, DOX, DOX and PM, and PM. Mitochondria showed vacuolization and loss of cristae after DOX treatment. Moreover, cardiomyocytes from DOX group showed disarranged myofilaments compared to the organized architecture in the CTRL group. PM treatment resulted in the amelioration of these structural changes. Furthermore, quantification of the mitochondria revealed that, compared to the CTRL, DOX decreased the mitochondrial density (P=0.0850), which was significantly increased after PM (P=0.0028; Fig. 2H top left panel). Moreover, treatment with PM alone showed a significant increase in mitochondrial density compared to the CTRL group (P<0.0001; Fig. 2H top left panel). Additionally, DOX significantly increased the cytoplasm fraction (P=0.0049; Fig. 2H bottom right panel). However, concomitant treatment with PM did not improve this parameter, but is significantly different from PM alone (P=0.0145; Fig. 2H bottom right panel). No significant differences were observed for the mitochondrial and myofilament fraction between the groups, as displayed in Fig. 2H (top right panel and bottom left panel).

DOX reduces LA7 cell viability and proliferation and increases cytotoxicity – To confirm the antitumor activity of DOX, LA7 cells were treated with increased concentrations of DOX for 24H, 48H, and 72H. As shown in Fig.3A and B, increasing concentrations of DOX reduced LA7 cell viability and proliferation, demonstrating the dose-dependent effect of DOX. After 24H, DOX concentrations higher than 0.5 µg/mL decreased the cell viability by more than 50% (Fig. 3A; 49.08% in 1 µg/mL, 40.37% in 1.75 µg/mL, 38.52% in 2.5 µg/mL, 34.62% in 5 µg/mL, and 32.14% in 10 µg/mL DOX). After 48H and 72H, the viability of LA7 cells was less than 20% for all DOX concentrations (Fig. 3A). Furthermore, DOX exposure reduced the proliferation of cells by more than 90% after 48H and 72H compared to DMEM (Fig. 3B). In line with these findings, cytotoxicity increased over time with increased DOX concentrations, further supporting the dose-dependent antitumor effect (Fig. 3C, 72H: 41 in DMEM, 482 in 0.5 µg/mL, 594 µg/mL in 1 µg/mL, 1185 in 1.75 µg/mL, 3023 in 2.5 µg/mL, 10056 in 5µg/mL, 17779 in 10 µg/mL).

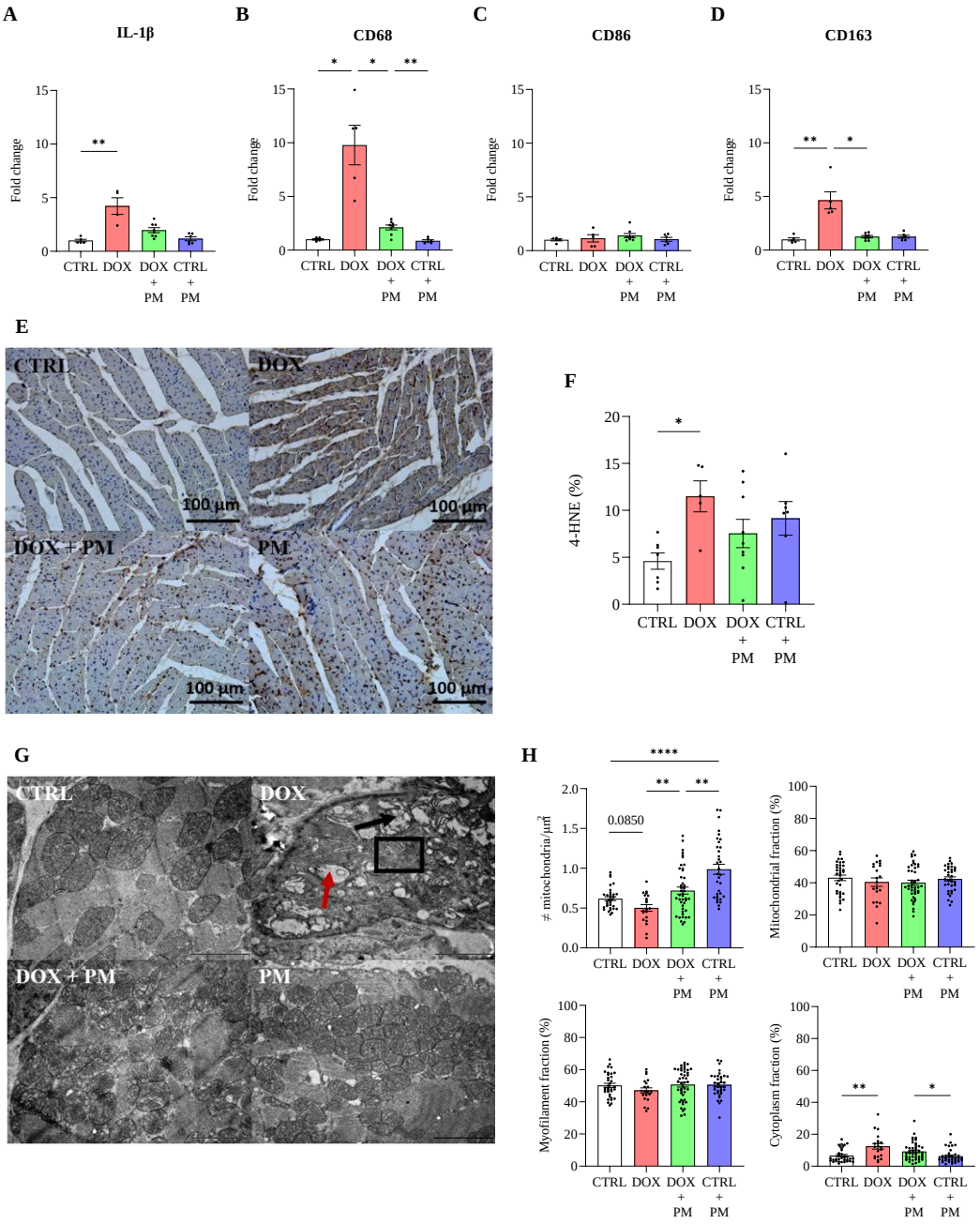

Figure 2: PM limits macrophage upregulation and mitochondrial damage after DOX. (A-D) Gene expression of the pro-inflammatory marker IL-1β **(A)**, the macrophage marker CD68 **(B)**, the M1 macrophage marker CD86 **(C)**, the M2a macrophage marker CD163 **(D)** in CTRL (N=5), DOX (N=5), DOX+PM (N=8) and PM (N=6) animals. Representative images **(E)** and quantification **(F)** of 4-HNE staining in LV tissue sections from CTRL (N=7), DOX (N=5), DOX+PM (N=9) and PM (N=7) animals. **(G)** Representative electron micrographs of the mitochondria in LV cardiomyocytes. In the DOX group, cardiomyocytes showed vacuolization of the mitochondria (red arrow), loss of cristae (black arrow), and disarranged myofilaments (black box), which were less evident in DOX+PM group. Magnification: 600x. Scale bars: 2 µm. **(H)** Quantification of the mitochondrial density, and percentage of mitochondrial, myofilament and cytoplasm fraction in cardiomyocytes from CTRL (N_{cells}=32-34), DOX (N_{cells}=20), DOX+PM (N_{cells}=44) and PM (N_{cells}=34-35) animals. Mitochondrial density is calculated as the ratio of mitochondrial number to total cell area. Intracellular fractions are expressed as a percentage of total grid points. Data are presented as mean ± SEM. *P<0.05, **P<0.01, ***P<0.001, ****P<0.0001. LV, left ventricular. IL-1β, interleukin 1 beta. 4-HNE, 4-hydroxynonenal.

PM does not interfere with the effect of DOX on LA7 cell viability and proliferation - To examine whether PM interferes with the antitumor activity of DOX, viability and proliferation of LA7 cells were measured after acute exposure to 1 µg/mL DOX, 100 µM PM or DOX and PM for 24H, 48H, and 72H. DOX significantly reduced LA7 cell viability ($P<0.0001$; Fig. 4A) and proliferation (24H: $P=0.005$; 48H and 72H: $P<0.0001$; Fig. 4B). Importantly, concomitant treatment with PM did not change the viability compared to DOX at all time points. In addition, the cell proliferation was not different between LA7 cells treated with DOX and DOX+PM, indicating PM does not interfere with the antitumor effect of DOX. Interestingly, PM treatment alone significantly reduced LA7 cell viability at 24H ($P=0.0085$) and 72H ($P=0.0395$), but did not change the proliferation (Fig. 4).

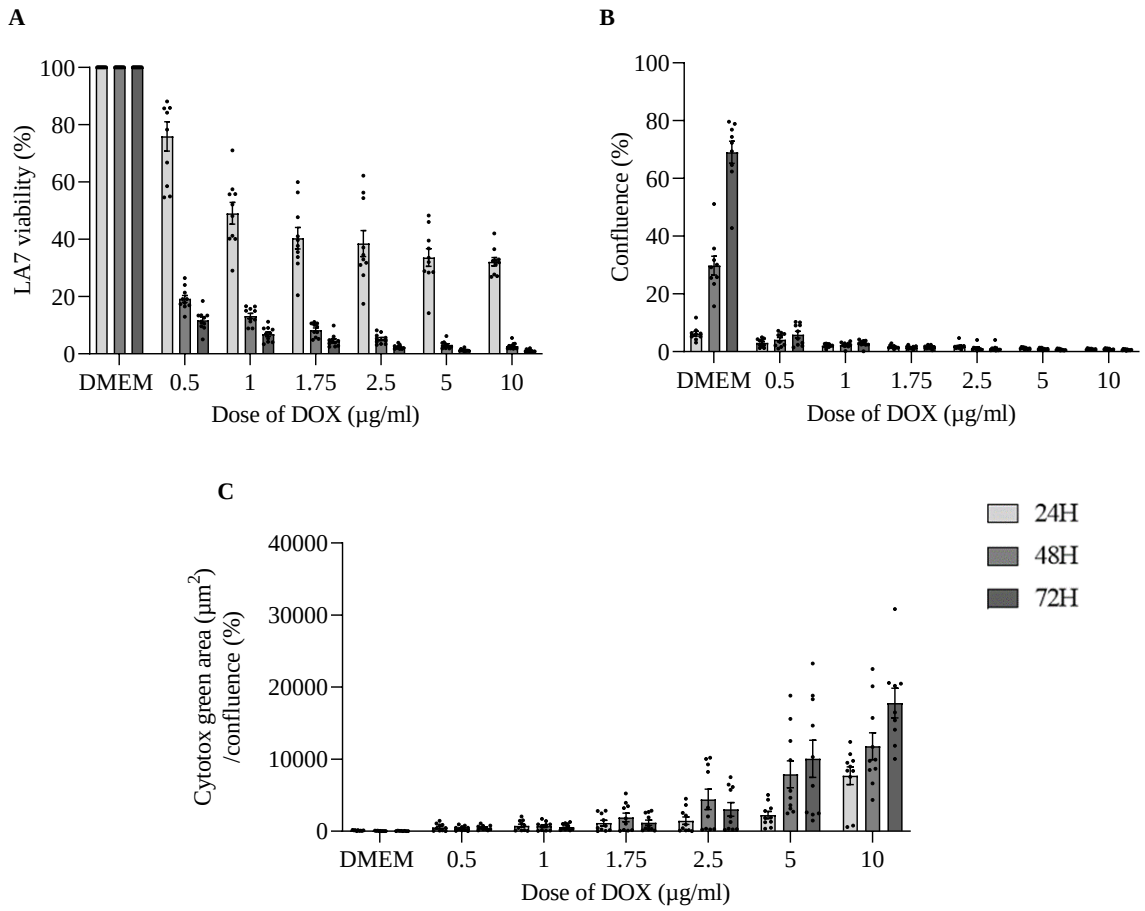

Figure 3: Increasing concentrations of DOX reduce LA7 cell viability and proliferation, and increase cytotoxicity after 24H, 48H and 72H exposure. (A-C) LA7 mammary tumor cells were exposed to different DOX concentrations (0.5, 1, 1.5, 1.75, 2.5, 5, 10 µg/ml). Cell viability **(A)**, proliferation, expressed as % confluence **(B)**, and cytotoxicity, expressed as the Cytotox green area (μm^2) divided by % confluence **(C)**, were measured after 24H, 48H and 72H (N=10 repetitions/group). Data are presented as mean ±SEM.

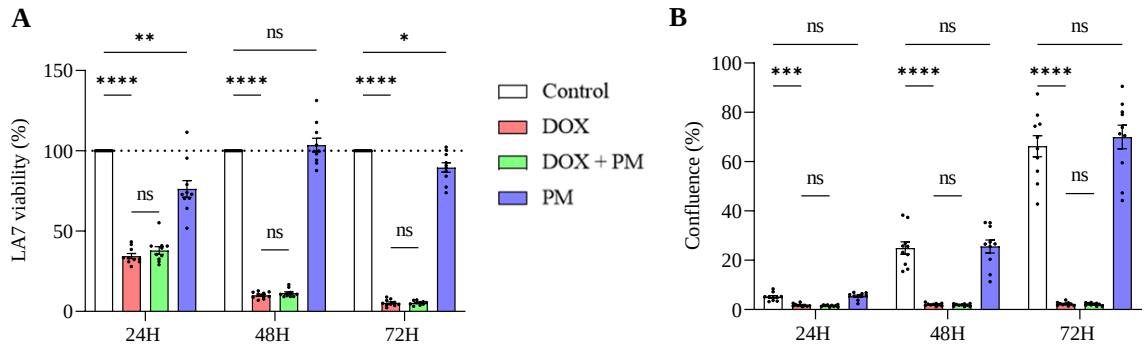

Figure 4: PM does not interfere with the effect of DOX on LA7 cell viability and proliferation. LA7 mammary tumor cells were exposed to DMEM (control), DOX (1 µg/mL), PM (100 µM) or DOX and PM. Cell viability **(A)** and proliferation, expressed as % confluence **(B)**, were measured after 24H, 48H and 72H (N=10 repetitions/group). Data are presented as mean ±SEM. *P<0.05, **P<0.01, ***P<0.001, ****P<0.0001.

PM does not affect the cytotoxic effect of DOX and DOX-induced apoptosis in LA7 cells – To investigate whether PM affects DOX efficacy, cytotoxicity was measured after acute exposure to 1 µg/mL DOX, 100 µM PM or DOX and PM for 24H, 48H, and 72H. As displayed in Fig. 5A, cytotoxicity was significantly increased after exposure to DOX after 48H and 72H (48H: P=0.035; 72H: P=0.0343). Importantly, concomitant treatment with PM did not affect the cytotoxic potency of DOX at 24H, 48H and 72H. PM alone showed no cytotoxic effects. Since cytotoxicity can result in apoptosis, cleaved caspase 3 fluorescence was measured after 24H. Compared to control, cleaved caspase 3 levels were significantly upregulated after DOX (P=0.0002; Fig. 5B). Interestingly, concomitant treatment with PM did not affect these cleaved caspase 3 levels, suggesting PM does not affect DOX-induced apoptosis (Fig. 5B). PM alone did not significantly increase cleaved caspase 3 levels, indicating no pro-apoptotic effect of PM.

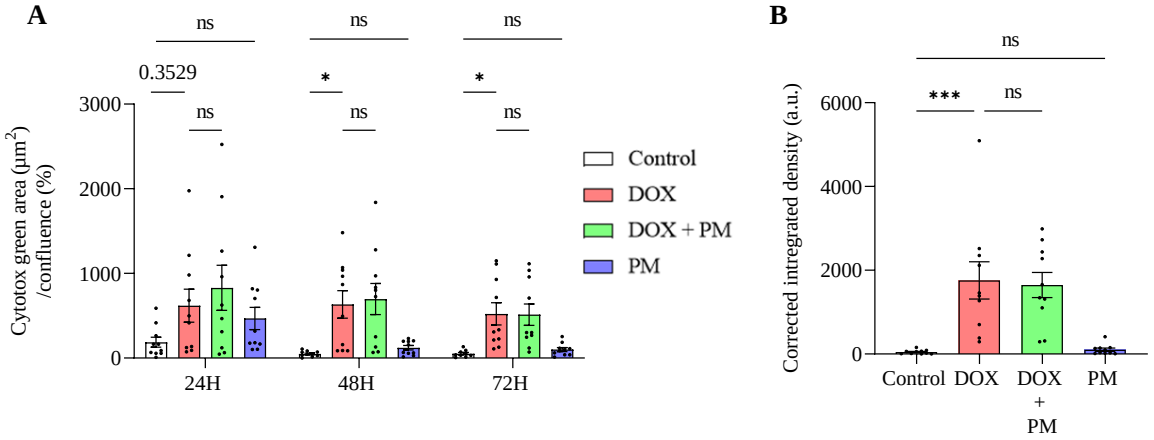

Figure 5: PM does not affect the cytotoxic effect of DOX and DOX-induced apoptosis in LA7 cells. LA7 mammary tumor cells were exposed to DMEM (control), DOX (1 µg/mL), PM (100 µM) or DOX and PM. Cytotoxicity **(A)**, expressed as the Cytotox green area (µm²) divided by % confluence, was measured after 24H, 48H and 72H (N=10 repetitions/group). Apoptosis **(B)**, expressed as corrected integrated density, was measured at 24H (N=10 repetitions/group). Data are presented as mean ±SEM. *P<0.05, ***P<0.001.

Optimization of the LA7-induced breast cancer rat model - To establish a translational breast cancer rat model for DOX-cardiotoxicity studies, female rats were inoculated with LA7 cells in the fourth mammary fat pad, as displayed in Table S2. Caliper measurements one week post-injection revealed a mean tumor volume of 415 mm^3, 365 mm^3 and 405 mm^3 in animals injected with $6x10^6$, $3x10^6$ or $4.5x10^6$ cells, respectively (Fig. 6A). However, no palpable tumor was observed after two weeks. To ensure the survival of LA7 cells after inoculation, LA7 cells resuspended in PBS or serum-free medium were injected in combination with growth factor-reduced Matrigel. After one week, the mean tumor volume was 624 mm^3 for animals injected with LA7 cells in PBS and 513 mm^3 for animals injected with LA7 cells in serum-free medium (Fig. 6B). Unfortunately, no palpable tumor could be detected two weeks after induction.

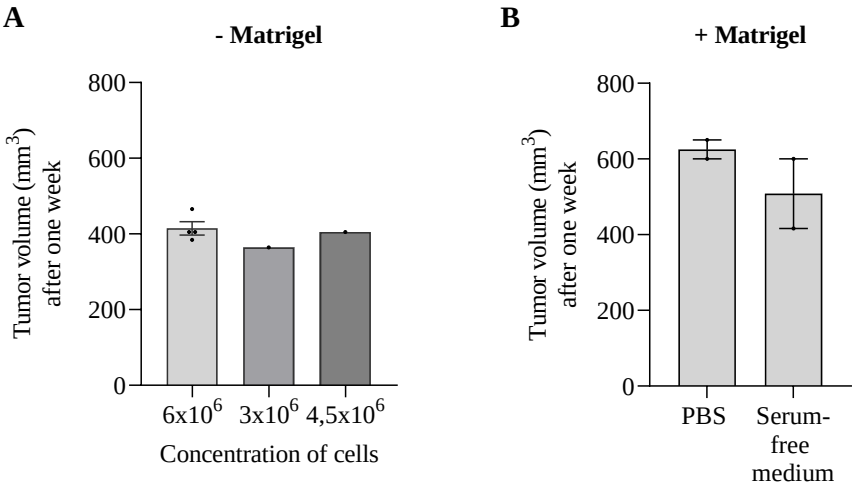

Figure 6: LA7 tumor cell injection results in a palpable mammary tumor one week post-injection. Female rats were inoculated with LA7 rat tumor cells subcutaneously in the fourth mammary fat pad without (N=6; concentration: $6x10^6$, $3x10^6$ or $4x10^6$ cells) **(A)** or with growth factor-reduced Matrigel (N=4; concentration: $6x10^6$ cells) **(B)**. Tumor volume was measured after one week with a digital caliper and calculated by multiplying the length of the tumor by the square of the width and dividing the product by two. Data are presented as mean ± SEM.

DISCUSSION

DOX is the most used anthracycline chemotherapy due to its efficacy in fighting a wide range of cancers including breast cancer. However, DOX also displays important toxic effects on the heart, affecting the patient's quality of life. PM has been demonstrated to limit DOX-induced cardiac dysfunction. In this study, we unravel the underlying cardioprotective mechanisms of PM. We show that PM prevents macrophage upregulation and mitochondrial damage in a tumor-lacking animal model. Due to the reciprocal relationship between HF and cancer, it is important to evaluate the effects of PM in a cancer setting. We show that PM does not antagonize the antitumor effects of DOX on the viability, proliferation, cytotoxicity and apoptosis of LA7 mammary tumor cells. Furthermore, we developed an LA7-induced breast cancer rat model.

Macrophage-driven inflammation, lipid peroxidation and mitochondrial damage contribute to DOX-induced cardiotoxicity

Healthy female Sprague-Dawley rats were weekly treated with DOX, PM, DOX and PM or a saline solution for eight weeks. A cumulative dose of 16 mg/kg DOX was applied, which is situated in the range of clinical DOX doses given in cancer patients (350-650 mg/mm^2) (2, 9). In our animal model, DOX induces dilated cardiomyopathy with systolic dysfunction, mimicking the clinical phenotype in DOX-treated patients. This indicates that our rat DOX cardiotoxicity model is valid and translatable. Preliminary findings from our research group indicate that DOX displays cardiac dysfunction through increased inflammation and oxidative stress, and disrupted iron regulation. To complement the findings on DOX-induced inflammation, macrophage markers and

macrophage subtypes were studied since macrophages contribute to inflammatory responses in CVDs. In DOX-treated animals, the pro-inflammatory marker IL-1β and the macrophage marker CD68 are increased, confirming the upregulation of macrophages in cardiac tissue of DOX-treated animals. Cardiac macrophages can originate from monocyte-derived macrophages or resident reparative macrophages. Zhang *et al.* (2020) reported that this upregulation may be induced through the proliferation of resident reparative macrophages (48). These macrophages express the scavenger receptor class A1 (SR-A1) for their regulation and reside in the cardiac tissue in a less alternatively activated state. In the presence of DOX, the SR-A1 expression is upregulated. SR-A1 can be activated by products of DOX-induced lipid peroxidation, resulting in the proliferation of these macrophages (48). These authors also demonstrated characteristic dynamic changes of macrophages during cardiac inflammation. The pro-inflammatory macrophages decline gradually four weeks after the start of DOX treatment, whereas reparative macrophages slowly increase along disease progression (48, 49). Accordingly, we show no upregulation of M1 macrophages after eight weeks of DOX treatment. Furthermore, the M2a macrophage marker CD163 was increased in DOX-treated animals, supporting the dominant role of reparative macrophages in the later phase of DOX-induced inflammation.

It has been recently demonstrated that mitochondrial iron accumulation plays an important role in DOX cardiotoxicity (50). DOX interacts with free transitional metals such as iron (Fe^{3+}), leading to the formation of unstable intracellular DOX-Fe^{3+} complexes. These complexes reduce Fe^{3+} to Fe^{2+} and oxidize DOX to the semiquinone radical, generating hydrogen peroxide and hydroxyl radical via the Fenton reaction (16, 51, 52). ROS react with polyunsaturated fatty acids (PUFAs) of the lipid membrane and induce lipid peroxidation (17). In this study, the extent of 4-HNE, a product generated from lipid peroxidation, was measured. We show that DOX increases 4-HNE levels in cardiac tissue, supporting the role of lipid peroxidation in DOX cardiotoxicity. Lipid peroxidation is known to drive ferroptosis, an iron-dependent programmed cell death (17-19). Fang *et al.* (2019) demonstrated that ferroptosis mediates chemotherapy-associated cardiotoxicity. They showed that DOX upregulates Hmox1, that is regulated by the transcription factor NRF2, which is also increased after DOX (Fig. 1D). Hmox1 degrades heme and releases free iron in cardiomyocytes, triggering lipid peroxidation and subsequent ferroptosis (19). Furthermore, previous studies reported that glutathione peroxidase 4 (GPx4), an endogenous scavenger for lipid peroxides, is a key regulator of ferroptosis. Tadokoro *et al.* (2020) showed that DOX downregulates GPx4 and that mitochondrial GPx4 overexpression prevents the progression of DOX-induced cardiotoxicity (52), suggests that targeting ferroptosis could limit DOX-induced cardiotoxicity. Since ferroptosis is mediated by mitochondrial iron accumulation and lipid peroxidation in the mitochondria, it is also characterized by compromised mitochondrial morphology (53). Mitochondria, highly abundant in cardiomyocytes, are the main subcellular target of DOX. DOX primarily redox cycles on complex 1, containing NADPH-dehydrogenase, of the electron transport chain. This results in the generation of ROS, which attacks the components of mitochondria. In addition, it has been described that DOX presents a strong affinity for cardiolipin, which is required for the activity of respiratory chain enzymes. DOX-cardiolipin complexes inhibit oxidative phosphorylation since cardiolipin can no longer act as cofactor for mitochondrial enzymes, leading to mitochondrial dysfunction (51, 52, 54). Therefore, DOX-treated animals are likely to display mitochondrial damage in cardiomyocytes, contributing to cardiac dysfunction. Indeed, our data show vacuolization of the mitochondria and loss of cristae and disarranged myofilaments. These findings are in accordance with previous research, indicating that DOX damages the ultrastructure of mitochondria (55-57). Furthermore, the mitochondrial density was decreased in DOX-treated animals. Taken together, our findings reveal that DOX disrupts iron regulation and induces oxidative stress, lipid peroxidation and mitochondrial damage, which collectively point toward the presence of ferroptosis in our model of DOX cardiotoxicity.

Effective cardioprotective strategies are lacking

During the last years, various cardiovascular drugs have been tested to prevent chemotherapy-induced cardiotoxicity. Two big clinical studies, the OVERCOME and the PRADA trial, combined a β-blocker and a renin–angiotensin

inhibitor to prevent cardiotoxicity in patients treated with anthracycline chemotherapy (58, 59). In the first trial, patients were administered carvedilol and lisinopril together at the start of chemotherapy, which was proven to be effective in preventing LVEF decline compared to the placebo (58). The PRADA trial investigated the combination of candesartan and metoprolol versus candesartan alone, metoprolol alone or placebo therapy. Breast cancer patients receiving candesartan during chemotherapy had less decline in LVEF. However metoprolol did not exhibit the same effect. Furthermore, there was no additional benefit when metoprolol was used with candesartan (59). Altogether, many cardioprotective strategies have been investigated, and, in some cases, yielded positive results. However, they have not demonstrated the ability to improve all parameters or significantly improve clinical outcomes (60-63). Further research is needed to develop more effective strategies for the comprehensive management of the disease and its impact on patient prognosis.

The underlying cardioprotective mechanisms of PM against DOX-induced cardiotoxicity

In this study, we focused on PM, a derivate of vitamin B6. Preliminary data from our research group has demonstrated that PM reduces the pro-inflammatory IL-6 levels in our DOX cardiotoxicity model. In addition, it has been evidenced that PM suppresses the pro-inflammatory cytokine IL-1β, suggesting anti-inflammatory properties of PM (64, 65). In contrast, our data did not show a significant reduction of IL-1β levels after PM treatment in our DOX cardiotoxicity model. This is consistent with the observations of Zhang *et al.* (2020), who demonstrate that other derivates of vitamin B6 reduced IL-1β production, but not PM specifically (66). Interestingly, we show that PM significantly alleviates the upregulation of macrophages, in particular M2a macrophages. Since the proliferation of resident reparative macrophages through SR-A1 activation contribute to DOX cardiotoxicity, these data suggest the ability of PM to modulate the immune response by suppressing SR-A1-mediated resident macrophage proliferation, which deserves further investigation.

It has been widely described that PM plays a key role in chelating metal ions, contributing to its antioxidant effects (67). Specifically, PM has been shown to form stable complexes with iron, reducing the availability of iron to form DOX-Fe^3 complexes. Indeed, preliminary data from our research group indicates that PM prevents the disturbance of iron regulation. By chelating iron, PM prevents the formation of ROS, suggesting the prevention of oxidative damage to lipid membranes and lipid peroxidation (67-69). Indeed, Jain *et al.* (2001) have shown that PM inhibits superoxide radical production and subsequent lipid peroxidation (70). In contrast, our data show that PM was not able to significantly reduce the lipid peroxidation-derived 4-HNE levels, indicating that the cardioprotective effects of PM are not mediated through the prevention of lipid peroxidation (71). In our study, we demonstrate that PM limits DOX-induced structural mitochondrial damage characterized by vacuolization and loss of cristae, and increases the mitochondrial density. It has been reported that DOX has a high affinity for the inner mitochondrial membrane component cardiolipin, accumulating in the mitochondria, resulting in mitochondrial dysfunction via different mechanisms (71). Whether PM has an effect on cardiolipin deserves further attention.

Taken together, PM prevents DOX-induced macrophage upregulation and partially protects against DOX-induced ferroptosis as evidenced by restored iron regulation and reduced mitochondrial damage, highlighting its promising cardioprotective nature.

The reciprocal relationship between HF and cancer

In preclinical studies investigating DOX cardiotoxicity and testing promising cardioprotective strategies, it is important to note that these have been conducted in healthy animals without tumors. While we also used a tumor-lacking animal model to study the cardioprotective effects of PM, we are working toward including a tumor model in our research. Recent studies have demonstrated a reciprocal relationship between HF and cancer. Emerging evidence supports that cancer incidence is increased in patients with HF, and patients with HF are more prone to develop cancer (43-45). This link can be explained by the shared risk factors (e.g., aging, smoking, genetic factors, diabetes mellitus) in combination with several common pathophysiological mechanisms, including inflammation and oxidative stress. Additionally, it has been demonstrated that circulating factors secreted by the injured heart promote tumor growth. Accordingly, De Boer *et al.* (2019) reported elevated levels of the pro-

tumor factors tumor necrosis factor-α, IL-6 and IL-1β in HF patients (45). Conversely, cancer cell-derived secreted factors can influence the development of HF. For example, cancer patients exhibit high levels of serum brain natriuretic peptide (BNP), a marker of HF (43). In summary, there is a tight interplay between HF and cancer, highlighting the importance of evaluating the cardioprotective effects of PM in a cancer setting.

DOX exhibits dose-dependent antitumor effects against LA7 mammary tumor cells and PM does not affect its efficacy

In the present study, we examined the *in vitro* effects of DOX and PM on viability, proliferation, cytotoxicity and apoptosis in rat mammary tumor cells to determine 1) the antitumor effects of DOX 2) whether PM interferes with DOX efficacy and 3) whether PM also exhibits antitumor effects itself. Since DOX is a common chemotherapeutic drug administered to breast cancer patients, we used the LA7 rat mammary tumor cells, derived from 7,12-dimethylbenz[a]anthracene (DMBA)-induced mammary tumors in Sprague-Dawley adult female rats. In this study, we tested increasing concentrations of DOX ranging from 0.5 to 10 µg/mL. These DOX concentrations are also used in other *in vitro* studies with DOX (72-75). We demonstrate a dose-dependent reduction in the viability and proliferation of LA7 cells. Additionally, we show enhanced cytotoxicity of these cells by increased concentrations of DOX. These findings confirm the efficacy of DOX on LA7 mammary tumor cells. Our data are in line with studies examining the effect of DOX on other breast cancer cells. Indeed, Nurhayati *et al.* (2020) demonstrated a dose-dependent decrease in the viability of MCF-7 human breast cancer cells, expressing estrogen and progesterone receptors, after exposure to DOX (76). The same effect of DOX on MCF-7 cell viability was observed by Aniogo *et al.* (2017) (77). In addition, they showed a dose-dependent reduction in cell proliferation (77). These data are further supported by Ubiyeye *et al.* (2019), who demonstrated decreased viability of MDA-MB-231 breast adenocarcinoma cells after exposure to increased DOX concentrations (72). It has been widely reported that the effect of DOX against cancer cells is mediated through intercalation into DNA and inhibition of Top2α. This enzyme is required for cell division during DNA transcription and replication. The inhibition of Top2α leads to double-stranded DNA breaks, resulting in apoptosis of the cancer cells (14, 15, 76, 78, 79). Indeed, apoptotic cell death after exposure to DOX is observed in various studies (72, 76, 77, 80). The generation of ROS, causing oxidative stress and subsequent apoptosis, has been proposed as another antitumor mechanism of DOX (14, 78). PM has been shown to protect against DOX-induced cardiotoxicity in a tumor-lacking animal model. Due to the reciprocal relationship between HF and cancer, the effects of PM need to be examined in a cancer setting. In this context, it is important to check whether PM affects the antitumor activity of DOX. Therefore, LA7 mammary tumor cells were acutely exposed to DOX, PM or a combination of DOX and PM. Based on previous experiments of DOX on cardiomyocytes, a concentration of 1 µg/mL DOX is used. Furthermore, analysis of plasma DOX in breast cancer patients revealed that the plasma concentration ranges between 0.01-0.6 µg/mL for cumulative doses between 48,76 and 319 mg/m^2, suggesting 1 µg/mL DOX corresponds to higher doses, which are used in breast cancer patients (81). Indeed, Sikora *et al.* (2022) reported that 1 µg/mL DOX in the peripheral blood corresponds to a dose of approximately 550 mg/m^2, suggesting a clinically relevant concentration of DOX (75). For PM, a concentration of 100 µM is applied based on other studies (82, 83). Our data showed that PM treatment combined with DOX does not change the effect of DOX on LA7 cell viability, proliferation, cytotoxicity and apoptosis. In line with these findings, a clinical trial showed that another vitamin B6 derivative, pyridoxine, has no impact on the antitumor effect of the chemotherapeutic drug capecitabine in patients with advanced colorectal or breast carcinoma (84). Galluzzi *et al.* (2012) further support the evidence that vitamin B6 does not affect chemotherapy efficacy in mice transplanted with Lewis lung carcinoma cells (85). Interestingly, we show that PM alone significantly reduced the viability after 24H and 72H, which may suggest antitumor effects of PM itself. Nevertheless, this hypothesis is disproved by our data demonstrating that PM has no effect on proliferation, cytotoxicity and apoptosis. Consistently, Matsuo *et al.* (2019) showed no antiproliferative activity of PM in HepG2 hepatoma cells and MKN45 gastric cancer cells (86). In addition, PM does not change the expression of the pro-apoptotic genes caspase 8 and BAX in SHSY5Y cells, confirming no effect of PM on apoptotic cell death (83).

Taken together, our data indicate that DOX is a highly effective chemotherapeutic drug against LA7 mammary tumor cells and that PM does not interfere with DOX efficacy.

LA7-induced mammary tumor rat model and future perspectives

In this study, we demonstrate a dose-dependent antitumor effect of DOX in LA7 mammary tumor cells. Importantly, PM does not affect DOX efficacy on LA7 cell viability, proliferation, cytotoxicity and apoptosis, providing the first evidence that PM is safe to use in combination with anticancer therapies. Hence, in a follow-up study, the effects of PM need to be evaluated in an LA7-induced tumor model treated with DOX. This will give insights into the cardioprotective effects of PM in a cancer setting. Since DOX is a commonly used chemotherapeutic agent in breast cancer treatment, a breast cancer rat model will be used to further mimic the clinical situation and to enhance the translatability to cancer patients. The most common methods to induce breast cancer include chemical agents (e.g., DMBA, MNU), which are time-consuming and have a long latency period (87, 88). Therefore, we use a short-term orthotopic method, involving the injection of LA7 cells into the mammary fat pad of rats. LA7 is a rat mammary tumor cell line with strong tumorigenic properties and a short latency period (87, 88). We developed an LA7-induced breast cancer rat model by injecting LA7 tumor cells alone or in combination with growth factor-reduced Matrigel. Consistent with other studies developing this tumor model, our data showed a tumor volume ranging from 360 to 600 mm^3 after one week of LA7 inoculation (87-90). Nevertheless, no palpable tumor could be detected after two weeks of tumor induction. This could be explained by an immune response against the tumor. Indeed, in this study, relatively young animals are used for tumor induction, that contain a large thymus. The thymus is responsible for the production and maturation of immune cells and declines in size during adult life, suggesting a higher immune response in our animals compared to older animals used in other studies (91). Hence, histological analysis of immune cell infiltration into the mammary fat pad needs to be performed in a future experiment. Besides the immune response, the lack of nutrients for tumor cell survival and growth could be another explanation. The use of growth factor-reduced Matrigel might not provide enough nutrients for tumor growth, indicating that high concentration Matrigel is required for LA7 tumor growth. In summary, optimization of the LA7 mammary tumor model using older animals and high-concentration Matrigel deserves further attention. Additionally, the cardioprotective effects of PM need to be investigated in this LA7-induced breast cancer model receiving DOX treatment. This may provide a novel cardioprotective strategy in DOX-treated cancer patients.

CONCLUSION

In conclusion, this study shows that macrophages drive DOX-induced inflammation, particularly M2a macrophages are prominent in the later phase of DOX-induced inflammation. Furthermore, our data demonstrate that DOX disrupts iron regulation and induces oxidative stress, lipid peroxidation and mitochondrial damage, which collectively point toward the presence of ferroptosis in our model of DOX cardiotoxicity. Importantly, PM is able to limit macrophage upregulation and partially protects against DOX-induced ferroptosis, further supporting its cardioprotective effects in DOX cardiotoxicity. In addition, we confirm the dose-dependent antitumor effects of DOX and show that DOX reduces LA7 cell viability and proliferation with a concomitant increase in cytotoxicity and apoptosis, indicating DOX efficacy in LA7 tumor cells. Importantly, concomitant treatment with PM did not alter the antitumor effects of DOX, which is promising for cancer patients suffering from cardiotoxicity. Finally, we demonstrate an LA7-induced breast cancer rat model, in which no palpable tumor could be detected after two weeks of tumor induction, that requires further optimization. In addition, a follow-up study needs to investigate whether PM is also an effective cardioprotective treatment in a preclinical cancer model in combination with DOX treatment.

REFERENCES

1. McGowan JV, Chung R, Maulik A, Piotrowska I, Walker JM, Yellon DM. Anthracycline Chemotherapy and Cardiotoxicity. Cardiovasc Drugs Ther. 2017;31(1):63-75.
2. Sung H, Ferlay J, Siegel RL, Laversanne M, Soerjomataram I, Jemal A, et al. Global Cancer Statistics 2020: GLOBOCAN Estimates of Incidence and Mortality Worldwide for 36 Cancers in 185 Countries. CA Cancer J Clin. 2021;71(3):209-49.
3. Sharma GN, Dave R, Sanadya J, Sharma P, Sharma KK. Various types and management of breast cancer: an overview. J Adv Pharm Technol Res. 2010;1(2):109-26.
4. Lukasiewicz S, Czeczelewski M, Forma A, Baj J, Sitarz R, Stanislawek A. Breast Cancer-Epidemiology, Risk Factors, Classification, Prognostic Markers, and Current Treatment Strategies-An Updated Review. Cancers (Basel). 2021;13(17).
5. Nardin S, Mora E, Varughese FM, D'Avanzo F, Vachanaram AR, Rossi V, et al. Breast Cancer Survivorship, Quality of Life, and Late Toxicities. Front Oncol. 2020;10:864.
6. Zhao M, Ding XF, Shen JY, Zhang XP, Ding XW, Xu B. Use of liposomal doxorubicin for adjuvant chemotherapy of breast cancer in clinical practice. J Zhejiang Univ Sci B. 2017;18(1):15-26.
7. Alexandre J, Cautela J, Ederhy S, Damaj GL, Salem JE, Barlesi F, et al. Cardiovascular Toxicity Related to Cancer Treatment: A Pragmatic Approach to the American and European Cardio-Oncology Guidelines. J Am Heart Assoc. 2020;9(18):e018403.
8. Swain SM, Whaley FS, Ewer MS. Congestive heart failure in patients treated with doxorubicin: a retrospective analysis of three trials. Cancer. 2003;97(11):2869-79.
9. Lopez-Sendon J, Alvarez-Ortega C, Zamora Aunon P, Buno Soto A, Lyon AR, Farmakis D, et al. Classification, prevalence, and outcomes of anticancer therapy-induced cardiotoxicity: the CARDIOTOX registry. Eur Heart J. 2020;41(18):1720-9.
10. Sturgeon KM, Deng L, Bluethmann SM, Zhou S, Trifiletti DM, Jiang C, et al. A population-based study of cardiovascular disease mortality risk in US cancer patients. Eur Heart J. 2019;40(48):3889-97.
11. Tocchetti CG, Ameri P, de Boer RA, D'Alessandra Y, Russo M, Sorriento D, et al. Cardiac dysfunction in cancer patients: beyond direct cardiomyocyte damage of anticancer drugs: novel cardio-oncology insights from the joint 2019 meeting of the ESC Working Groups of Myocardial Function and Cellular Biology of the Heart. Cardiovasc Res. 2020;116(11):1820-34.
12. Kourek C, Touloupaki M, Rempakos A, Loritis K, Tsougkos E, Paraskevaidis I, et al. Cardioprotective Strategies from Cardiotoxicity in Cancer Patients: A Comprehensive Review. J Cardiovasc Dev Dis. 2022;9(8).
13. Chatterjee K, Zhang J, Honbo N, Karliner JS. Doxorubicin cardiomyopathy. Cardiology. 2010;115(2):155-62.
14. Henriksen PA. Anthracycline cardiotoxicity: an update on mechanisms, monitoring and prevention. Heart. 2018;104(12):971-7.
15. Songbo M, Lang H, Xinyong C, Bin X, Ping Z, Liang S. Oxidative stress injury in doxorubicin-induced cardiotoxicity. Toxicol Lett. 2019;307:41-8.
16. Kwok JC, Richardson DR. The cardioprotective effect of the iron chelator dexrazoxane (ICRF-187) on anthracycline-mediated cardiotoxicity. Redox Rep. 2000;5(6):317-24.
17. Rochette L, Dogon G, Rigal E, Zeller M, Cottin Y, Vergely C. Lipid Peroxidation and Iron Metabolism: Two Corner Stones in the Homeostasis Control of Ferroptosis. Int J Mol Sci. 2022;24(1).
18. Dixon SJ, Lemberg KM, Lamprecht MR, Skouta R, Zaitsev EM, Gleason CE, et al. Ferroptosis: an iron-dependent form of nonapoptotic cell death. Cell. 2012;149(5):1060-72.
19. Fang X, Wang H, Han D, Xie E, Yang X, Wei J, et al. Ferroptosis as a target for protection against cardiomyopathy. Proc Natl Acad Sci U S A. 2019;116(7):2672-80.
20. Cappetta D, De Angelis A, Sapio L, Prezioso L, Illiano M, Quaini F, et al. Oxidative Stress and Cellular Response to Doxorubicin: A Common Factor in the Complex Milieu of Anthracycline Cardiotoxicity. Oxid Med Cell Longev. 2017;2017:1521020.
21. Wang S, Kotamraju S, Konorev E, Kalivendi S, Joseph J, Kalyanaraman B. Activation of nuclear factor-kappaB during doxorubicin-induced apoptosis in endothelial cells and myocytes is pro-apoptotic: the role of hydrogen peroxide. Biochem J. 2002;367(Pt 3):729-40.

22. Sadek KM, Mahmoud SFE, Zeweil MF, Abouzed TK. Proanthocyanidin alleviates doxorubicin-induced cardiac injury by inhibiting NF-kB pathway and modulating oxidative stress, cell cycle, and fibrogenesis. J Biochem Mol Toxicol. 2021;35(4):e22716.
23. Cardinale D, Iacopo F, Cipolla CM. Cardiotoxicity of Anthracyclines. Front Cardiovasc Med. 2020;7:26.
24. Rivankar S. An overview of doxorubicin formulations in cancer therapy. J Cancer Res Ther. 2014;10(4):853-8.
25. Paiva MG, Petrilli AS, Moises VA, Macedo CR, Tanaka C, Campos O. Cardioprotective effect of dexrazoxane during treatment with doxorubicin: a study using low-dose dobutamine stress echocardiography. Pediatr Blood Cancer. 2005;45(7):902-8.
26. Macedo AVS, Hajjar LA, Lyon AR, Nascimento BR, Putzu A, Rossi L, et al. Efficacy of Dexrazoxane in Preventing Anthracycline Cardiotoxicity in Breast Cancer. JACC CardioOncol. 2019;1(1):68-79.
27. Shaikh F, Dupuis LL, Alexander S, Gupta A, Mertens L, Nathan PC. Cardioprotection and Second Malignant Neoplasms Associated With Dexrazoxane in Children Receiving Anthracycline Chemotherapy: A Systematic Review and Meta-Analysis. J Natl Cancer Inst. 2016;108(4).
28. Reichardt P, Tabone MD, Mora J, Morland B, Jones RL. Risk-benefit of dexrazoxane for preventing anthracycline-related cardiotoxicity: re-evaluating the European labeling. Future Oncol. 2018;14(25):2663-76.
29. Chow EJ, Aplenc R, Vrooman LM, Doody DR, Huang YV, Aggarwal S, et al. Late health outcomes after dexrazoxane treatment: A report from the Children's Oncology Group. Cancer. 2022;128(4):788-96.
30. Jones RL, Wagner AJ, Kawai A, Tamura K, Shahir A, Van Tine BA, et al. Prospective Evaluation of Doxorubicin Cardiotoxicity in Patients with Advanced Soft-tissue Sarcoma Treated in the ANNOUNCE Phase III Randomized Trial. Clin Cancer Res. 2021;27(14):3861-6.
31. Li J, Chang HM, Banchs J, Araujo DM, Hassan SA, Wagar EA, et al. Detection of subclinical cardiotoxicity in sarcoma patients receiving continuous doxorubicin infusion or pre-treatment with dexrazoxane before bolus doxorubicin. Cardiooncology. 2020;6:1.
32. Proskuriakova E, Jada K, Kakieu Djossi S, Khedr A, Neupane B, Mostafa JA. Mechanisms and Potential Treatment Options of Heart Failure in Patients With Multiple Myeloma. Cureus. 2021;13(6):e15943.
33. Stansfeld A, Radia U, Goggin C, Mahalingam P, Benson C, Napolitano A, et al. Pharmacological strategies to reduce anthracycline-associated cardiotoxicity in cancer patients. Expert Opin Pharmacother. 2022;23(14):1641-50.
34. Van Tine BA, Hirbe AC, Oppelt P, Frith AE, Rathore R, Mitchell JD, et al. Interim Analysis of the Phase II Study: Noninferiority Study of Doxorubicin with Upfront Dexrazoxane plus Olaratumab for Advanced or Metastatic Soft-Tissue Sarcoma. Clin Cancer Res. 2021;27(14):3854-60.
35. Stach K, Stach W, Augoff K. Vitamin B6 in Health and Disease. Nutrients. 2021;13(9).
36. Jeon J, Park K. Dietary Vitamin B(6) Intake Associated with a Decreased Risk of Cardiovascular Disease: A Prospective Cohort Study. Nutrients. 2019;11(7).
37. Friso S, Jacques PF, Wilson PW, Rosenberg IH, Selhub J. Low circulating vitamin B(6) is associated with elevation of the inflammation marker C-reactive protein independently of plasma homocysteine levels. Circulation. 2001;103(23):2788-91.
38. Kumrungsee T, Peipei Z, Yanaka N, Suda T, Kato N. Emerging cardioprotective mechanisms of vitamin B6: a narrative review. Eur J Nutr. 2022;61(2):605-13.
39. Yanaka N, Koyama TA, Komatsu S, Nakamura E, Kanda M, Kato N. Vitamin B6 suppresses NF-kappaB activation in LPS-stimulated mouse macrophages. Int J Mol Med. 2005;16(6):1071-5.
40. Suidasari S, Stautemas J, Uragami S, Yanaka N, Derave W, Kato N. Carnosine Content in Skeletal Muscle Is Dependent on Vitamin B6 Status in Rats. Front Nutr. 2015;2:39.
41. Suidasari S, Hasegawa T, Yanaka N, Kato N. Dietary supplemental vitamin B6 increases carnosine and anserine concentrations in the heart of rats. Springerplus. 2015;4:280.
42. Deluyker D, Ferferieva V, Driesen RB, Verboven M, Lambrichts I, Bito V. Pyridoxamine improves survival and limits cardiac dysfunction after MI. Sci Rep. 2017;7(1):16010.
43. Guler MN, Tscheiller NM, Sabater-Molina M, Gimeno JR, Nebigil CG. Evidence for reciprocal network interactions between injured hearts and cancer. Front Cardiovasc Med. 2022;9:929259.

44. Bertero E, Ameri P, Maack C. Bidirectional Relationship Between Cancer and Heart Failure: Old and New Issues in Cardio-oncology. Card Fail Rev. 2019;5(2):106-11.
45. de Boer RA, Meijers WC, van der Meer P, van Veldhuisen DJ. Cancer and heart disease: associations and relations. Eur J Heart Fail. 2019;21(12):1515-25.
46. Bustin SA, Benes V, Garson JA, Hellemans J, Huggett J, Kubista M, et al. The MIQE guidelines: minimum information for publication of quantitative real-time PCR experiments. Clin Chem. 2009;55(4):611-22.
47. Schindelin J, Arganda-Carreras I, Frise E, Kaynig V, Longair M, Pietzsch T, et al. Fiji: an open-source platform for biological-image analysis. Nat Methods. 2012;9(7):676-82.
48. Zhang H, Xu A, Sun X, Yang Y, Zhang L, Bai H, et al. Self-Maintenance of Cardiac Resident Reparative Macrophages Attenuates Doxorubicin-Induced Cardiomyopathy Through the SR-A1-c-Myc Axis. Circ Res. 2020;127(5):610-27.
49. Burridge PW, Thorp EB. Doxorubicin-Induced Ascension of Resident Cardiac Macrophages. Circ Res. 2020;127(5):628-30.
50. Ichikawa Y, Ghanefar M, Bayeva M, Wu R, Khechaduri A, Naga Prasad SV, et al. Cardiotoxicity of doxorubicin is mediated through mitochondrial iron accumulation. J Clin Invest. 2014;124(2):617-30.
51. Carvalho FS, Burgeiro A, Garcia R, Moreno AJ, Carvalho RA, Oliveira PJ. Doxorubicin-induced cardiotoxicity: from bioenergetic failure and cell death to cardiomyopathy. Med Res Rev. 2014;34(1):106-35.
52. Tadokoro T, Ikeda M, Ide T, Deguchi H, Ikeda S, Okabe K, et al. Mitochondria-dependent ferroptosis plays a pivotal role in doxorubicin cardiotoxicity. JCI Insight. 2020;5(9).
53. Wu H, Wang F, Ta N, Zhang T, Gao W. The Multifaceted Regulation of Mitochondria in Ferroptosis. Life (Basel). 2021;11(3).
54. Guo Q, Guo J, Yang R, Peng H, Zhao J, Li L, et al. Cyclovirobuxine D Attenuates Doxorubicin-Induced Cardiomyopathy by Suppression of Oxidative Damage and Mitochondrial Biogenesis Impairment. Oxid Med Cell Longev. 2015;2015:151972.
55. Abdelatty A, Ahmed MS, Abdel-Kareem MA, Dmerdash M, Mady R, Saad AS, et al. Acute and Delayed Doxorubicin-Induced Myocardiotoxicity Associated with Elevation of Cardiac Biomarkers, Depletion of Cellular Antioxidant Enzymes, and Several Histopathological and Ultrastructural Changes. Life (Basel). 2021;11(9).
56. Al-Harthi SE, Alarabi OM, Ramadan WS, Alaama MN, Al-Kreathy HM, Damanhouri ZA, et al. Amelioration of doxorubicin-induced cardiotoxicity by resveratrol. Mol Med Rep. 2014;10(3):1455-60.
57. Li L, Ni J, Li M, Chen J, Han L, Zhu Y, et al. Ginsenoside Rg3 micelles mitigate doxorubicin-induced cardiotoxicity and enhance its anticancer efficacy. Drug Deliv. 2017;24(1):1617-30.
58. Bosch X, Rovira M, Sitges M, Domenech A, Ortiz-Perez JT, de Caralt TM, et al. Enalapril and carvedilol for preventing chemotherapy-induced left ventricular systolic dysfunction in patients with malignant hemopathies: the OVERCOME trial (preventiOn of left Ventricular dysfunction with Enalapril and caRvedilol in patients submitted to intensive ChemOtherapy for the treatment of Malignant hEmopathies). J Am Coll Cardiol. 2013;61(23):2355-62.
59. Gulati G, Heck SL, Ree AH, Hoffmann P, Schulz-Menger J, Fagerland MW, et al. Prevention of cardiac dysfunction during adjuvant breast cancer therapy (PRADA): a 2 x 2 factorial, randomized, placebo-controlled, double-blind clinical trial of candesartan and metoprolol. Eur Heart J. 2016;37(21):1671-80.
60. Gupta V, Kumar Singh S, Agrawal V, Bali Singh T. Role of ACE inhibitors in anthracycline-induced cardiotoxicity: A randomized, double-blind, placebo-controlled trial. Pediatr Blood Cancer. 2018;65(11):e27308.
61. He D, Hu J, Li Y, Zeng X. Preventive use of beta-blockers for anthracycline-induced cardiotoxicity: A network meta-analysis. Front Cardiovasc Med. 2022;9:968534.
62. Ma Y, Bai F, Qin F, Li J, Liu N, Li D, et al. Beta-blockers for the primary prevention of anthracycline-induced cardiotoxicity: a meta-analysis of randomized controlled trials. BMC Pharmacol Toxicol. 2019;20(1):18.

63. Vaduganathan M, Hirji SA, Qamar A, Bajaj N, Gupta A, Zaha V, et al. Efficacy of Neurohormonal Therapies in Preventing Cardiotoxicity in Patients with Cancer Undergoing Chemotherapy. JACC CardioOncol. 2019;1(1):54-65.
64. Li J, Jeong SY, Xiong B, Tseng A, Mahon AB, Isaacman S, et al. Repurposing pyridoxamine for therapeutic intervention of intravascular cell-cell interactions in mouse models of sickle cell disease. Haematologica. 2020;105(10):2407-19.
65. Zhang X, Xu L, Chen W, Yu X, Shen L, Huang Y. Pyridoxamine alleviates mechanical allodynia by suppressing the spinal receptor for advanced glycation end product-nuclear factor-kappaB/extracellular signal-regulated kinase signaling pathway in diabetic rats. Mol Pain. 2020;16:1744806920917251.
66. Zhang P, Tsuchiya K, Kinoshita T, Kushiyama H, Suidasari S, Hatakeyama M, et al. Vitamin B6 Prevents IL-1beta Protein Production by Inhibiting NLRP3 Inflammasome Activation. J Biol Chem. 2016;291(47):24517-27.
67. Ramis R, Ortega-Castro J, Caballero C, Casasnovas R, Cerrillo A, Vilanova B, et al. How Does Pyridoxamine Inhibit the Formation of Advanced Glycation End Products? The Role of Its Primary Antioxidant Activity. Antioxidants (Basel). 2019;8(9).
68. Adrover M, Vilanova B, Frau J, Munoz F, Donoso J. The pyridoxamine action on Amadori compounds: A reexamination of its scavenging capacity and chelating effect. Bioorg Med Chem. 2008;16(10):5557-69.
69. Garcia-Diez G, Monreal-Corona R, Mora-Diez N. Complexes of Copper and Iron with Pyridoxamine, Ascorbic Acid, and a Model Amadori Compound: Exploring Pyridoxamine's Secondary Antioxidant Activity. Antioxidants (Basel). 2021;10(2).
70. Jain SK, Lim G. Pyridoxine and pyridoxamine inhibits superoxide radicals and prevents lipid peroxidation, protein glycosylation, and (Na+ + K+)-ATPase activity reduction in high glucose-treated human erythrocytes. Free Radic Biol Med. 2001;30(3):232-7.
71. Wallace KB, Sardao VA, Oliveira PJ. Mitochondrial Determinants of Doxorubicin-Induced Cardiomyopathy. Circ Res. 2020;126(7):926-41.
72. Ibiyeye KM, Nordin N, Ajat M, Zuki ABZ. Ultrastructural Changes and Antitumor Effects of Doxorubicin/Thymoquinone-Loaded CaCO(3) Nanoparticles on Breast Cancer Cell Line. Front Oncol. 2019;9:599.
73. Janssen FP, Bouten CV, van Leeuwen GM, van Steenhoven AA. Effects of temperature and doxorubicin exposure on keratinocyte damage in vitro. In Vitro Cell Dev Biol Anim. 2008;44(3-4):81-6.
74. Sharma A, Ozayral S, Caserto JS, Ten Cate R, Anders NM, Barnett JD, et al. Increased uptake of doxorubicin by cells undergoing heat stress does not explain its synergistic cytotoxicity with hyperthermia. Int J Hyperthermia. 2019;36(1):712-20.
75. Sikora T, Morawska K, Lisowski W, Rytel P, Dylong A. Application of Optical Methods for Determination of Concentration of Doxorubicin in Blood and Plasma. Pharmaceuticals (Basel). 2022;15(2).
76. Nurhayati IP, Khumaira A, Ilmawati GPN, Meiyanto E, Hermawan A. Cytotoxic and Antimetastatic Activity of Hesperetin and Doxorubicin Combination Toward Her2 Expressing Breast Cancer Cells. Asian Pac J Cancer Prev. 2020;21(5):1259-67.
77. Aniogo EC, George BPA, Abrahamse H. In vitro combined effect of Doxorubicin and sulfonated zinc Phthalocyanine-mediated photodynamic therapy on MCF-7 breast cancer cells. Tumour Biol. 2017;39(10):1010428317727278.
78. Taymaz-Nikerel H, Karabekmez ME, Eraslan S, Kirdar B. Doxorubicin induces an extensive transcriptional and metabolic rewiring in yeast cells. Sci Rep. 2018;8(1):13672.
79. Nitiss JL. Targeting DNA topoisomerase II in cancer chemotherapy. Nat Rev Cancer. 2009;9(5):338-50.
80. Lupertz R, Watjen W, Kahl R, Chovolou Y. Dose- and time-dependent effects of doxorubicin on cytotoxicity, cell cycle and apoptotic cell death in human colon cancer cells. Toxicology. 2010;271(3):115-21.
81. Harahap Y, Ardiningsih P, Corintias Winarti A, Purwanto DJ. Analysis of the Doxorubicin and Doxorubicinol in the Plasma of Breast Cancer Patients for Monitoring the Toxicity of Doxorubicin. Drug Des Devel Ther. 2020;14:3469-75.

82. Jiang M, Yakupu A, Guan H, Dong J, Liu Y, Song F, et al. Pyridoxamine ameliorates methylglyoxal-induced macrophage dysfunction to facilitate tissue repair in diabetic wounds. Int Wound J. 2022;19(1):52-63.
83. Vrolijk MF, Opperhuizen A, Jansen E, Hageman GJ, Bast A, Haenen G. The vitamin B6 paradox: Supplementation with high concentrations of pyridoxine leads to decreased vitamin B6 function. Toxicol In Vitro. 2017;44:206-12.
84. Corrie PG, Bulusu R, Wilson CB, Armstrong G, Bond S, Hardy R, et al. A randomised study evaluating the use of pyridoxine to avoid capecitabine dose modifications. Br J Cancer. 2012;107(4):585-7.
85. Galluzzi L, Vitale I, Senovilla L, Olaussen KA, Pinna G, Eisenberg T, et al. Prognostic impact of vitamin B6 metabolism in lung cancer. Cell Rep. 2012;2(2):257-69.
86. Matsuo T, Sadzuka Y. In Vitro Anticancer Activities of B(6) Vitamers: A Mini-review. Anticancer Res. 2019;39(7):3429-32.
87. Abbasalipourkabir R DA, Salehzadeh A, Shamsabadi F, Abdullah R. Induction of mammary gland tumor in female Sprague Dawley rats with LA7 cells. African Journal of Biotechnology. 2010.
88. Oyenihi OR, Krygsman A, Verhoog N, de Beer D, Saayman MJ, Mouton TM, et al. Chemoprevention of LA7-Induced Mammary Tumor Growth by SM6Met, a Well-Characterized Cyclopia Extract. Front Pharmacol. 2018;9:650.
89. Karimian H, Fadaeinasab M, Zorofchian Moghadamtousi S, Hajrezaei M, Razavi M, Safi SZ, et al. Chemopreventive Activity of Ferulago angulate against Breast Tumor in Rats and the Apoptotic Effect of Polycerasoidin in MCF7 Cells: A Bioassay-Guided Approach. PLoS One. 2015;10(5):e0127434.
90. Mehri M, Gheitasi R, Pourbagher R, Ranaee M, Nayeri K, Rahimi SM, et al. Ninety-six-hour starved peripheral blood mononuclear cell supernatant inhibited LA7 breast cancer stem cells induced tumor via reduction in angiogenesis and alternations in Gch1 and Spr expressions. Front Immunol. 2022;13:1025933.
91. Shichkin VP, Antica M. Key Factors for Thymic Function and Development. Front Immunol. 2022;13:926516.

Acknowledgements – I thank S.H. for the guidance through both my project and the writing of my master's thesis. I am especially grateful for S.H. support and confidence in me during the entire process. His guidance and support have been important in my personal and academic growth. I also thank the whole cardiology research team (V.B, D. D., S.D.H., E.H.) for welcoming me in their team. Being a part of this team has been a valuable experience and I am grateful for the opportunity to have worked with them. In addition, I thank Wendy Vandendries for assisting with the transmission electron microscope. I also thank Jolien Van Den Bosch for the growth-factor reduced Matrigel. Finally, I thank Petra Bex and Evelyne Vankerckhove for their skillful technical assistance, and Melissa Jans and Yennick Geuens for animal housing.

Author contributions – V.B., E.W., D.D., and S.H. conceived and designed the research. D.D., S.H., and E.V. performed experiments and data analysis. D.D. and S.H. provided assistance with the execution of the experiments. E.V. wrote the paper. S.H. critically reviewed the manuscript.

SUPPLEMENTARY MATERIALS, TABLES AND FIGURES

Supplementary Materials

Mammary tumor induction – Sprague-Dawley female rats (±150g, N=10, Charles River Laboratories, L'Arbresle, France) were subjected to LA7 mammary tumor induction. The rats were anesthetized using 2% isoflurane and 0.02 mg/kg Buprenorphine (0.3 mg/mL) was administered intramuscularly as pain medication. The injection site was properly cleaned and sterilized with isobetadine and ethanol. The cell suspension was inoculated subcutaneously into the fourth mammary fat pad (right flank) of the Sprague Dawley rats using a 1 mL TB syringe with #26 gauge needle. Rats were injected with $6x10^6$ cells (N=4), $3x10^6$ cells (N=1) and $4.5x10^6$ cells (N=1) resuspended in 300 µl 1xPBS. Rats were injected with $6x10^6$ cells resuspended in 50 µl 1xPBS (N=2) or serum-free medium (N=2) and 50µl growth factor-reduced Matrigel (Corning, Lasne, Belgium). The areas surrounding the injection site were washed with PBS to dissipate any cells that may have spilled or leaked. The skin was occluded with 5.0 Vicryl Rapide suture. After two, three or four weeks, the rats were sacrificed and the fourth mammary fat pad was harvested, fixed in 4% PFA and embedded in paraffin. Transverse sections of 7 µm were obtained.

Tumor measurement – For tumor volume estimation, the tumor's length and width were measured using a digital caliper. Tumor volume was calculated by the following formula: (length x $width^2$)/2 (88).

Supplementary Tables

Table S1: Primer sequences used for qPCR.

	Forward primer (5'→3')	**Reverse primer (3'→5')**
	Reference genes	
Tbp	TGGGATTGTACCACAGCTCCA	CTCATGATGACTGCAGCAAACC
Rpl13a	GGATCCCTCCACCCTATGACA	CTGGTACTTCCACCCGACCTC
	Target genes	
IL-1β	ACC CAA GCA CCT TCT TTT CCT T	TGC AGC TGT CTA ATG GGA ACA T
CD68	ATCACAGCATGGCACAGGT	TCCAGATCATCCGTCTTCG
CD86	GTCAAGACATGTGTAACCTGCACC	ACGAGCTCACTCGGGCTTAT
CD206	TCCCTCAATGGAACACACACTC	TTAAAAATTGCCGTGAGTCCAAGAG
CD163	CACTTGGCTCTCTCATTCCCT	GCTGAGAATGTCCACTGTGCT

Tbp, TATA box binding protein. Rpl13a, Ribosomal protein L13a. IL-1β, interleukin-1 beta. CD206, mannose receptor C-type I.

Table S2: Additional information on the mammary tumor induction.

Rat	**LA7 cell concentration**	**Matrigel?**	**PBS or serum-free medium?**	**Tumor volume (mm^3)**
1	6×10^6	No	PBS	465.75
2	6×10^6	No	PBS	384
3	3×10^6	No	PBS	364.5
4	4.5×10^6	No	PBS	405
5	6×10^6	No	PBS	405
6	6×10^6	No	PBS	405
7	6×10^6	Yes	PBS	650
8	6×10^6	Yes	Serum-free medium	416
9	6×10^6	Yes	PBS	600
10	6×10^6	Yes	Serum-free medium	600

Supplementary Results

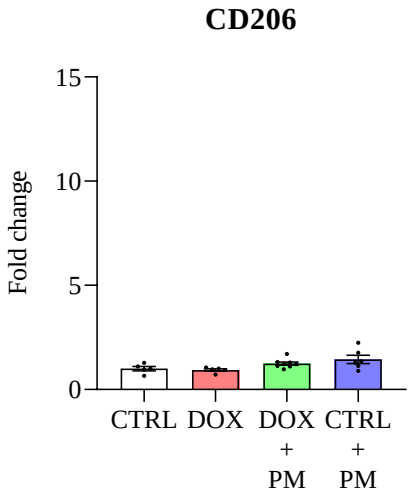

Figure S1: DOX and PM did not change CD206 expression. Gene expression of the M2a macrophage marker CD206 in CTRL (N=5), DOX (N=5), DOX+PM (N=8) and PM (N=6) rats. Data are presented as mean ± SEM.